Three dimensional cooling and trapping with a narrow line

Thierry Chaneliere, Ling Xiang He, Robin Kaiser, David Wilkowski

EPJ manuscript No.
(will be inserted by the editor)

Three dimensional cooling and trapping with a narrow line

T. Chanelière[1], L. He[2], R. Kaiser[3] and D. Wilkowski[3]

[1] + Now at: Laboratoire Aimé Cotton, CNRS, UPR 3321, Université Paris-Sud, Bat. 505, F-91405 Orsay Cedex, France
[2] * Now at: State Key Laboratory of Magnetic Resonance and Atomic and Molecular Wuhan Institute of Physics and Mathematics, Chinese Academy of Sciences, Wuhan 430071, P. R. China
[3] Institut Non Linéaire de Nice, CNRS, UMR 6618, Université de Nice Sophia-Antipolis, F-06560 Valbonne, France.

August 10, 2007

Abstract. The intercombination line of Strontium at 689nm is successfully used in laser cooling to reach the photon recoil limit with Doppler cooling in a magneto-optical traps (MOT). In this paper we present a systematic study of the loading efficiency of such a MOT. Comparing the experimental results to a simple model allows us to discuss the actual limitation of our apparatus. We also study in detail the final MOT regime emphasizing the role of gravity on the position, size and temperature along the vertical and horizontal directions. At large laser detuning, one finds an unusual situation where cooling and trapping occur in the presence of a high bias magnetic field.

PACS. 3 9.25.+k

1 Introduction

Cooling and trapping alkaline-earth atoms offer interesting alternatives to alkaline atoms. Indeed, the singlet-triplet forbidden lines can be used for optical frequency measurement and related subjects [1]. Moreover, the spinless ground state of the most abundant bosonic isotopes can lead to simpler or at least different cold collisions problems than with alkaline atoms [2]. Considering fermionic isotopes, the long-living and isolated nuclear spin can be controlled by optical means [3] and has been proposed to implement quantum logic gates [4]. It has also been shown that the ultimate performance of Doppler cooling can be greatly improved by using narrow transitions whose photon recoil frequency shifts ω_r are larger than their natural widths Γ [5]. This is the case for the ${}^1S_0 \rightarrow {}^3P_1$ spin-forbidden line of Magnesium ($\omega_r \approx 1100\Gamma$) or Calcium ($\omega_r \approx 36\Gamma$). Unfortunately, both atomic species can not be hold in a standard magneto-optical trap (MOT) because the radiation pressure force is not strong enough to overcome gravity. This imposes the use of an extra quenching laser as demonstrated for Ca [6]. For Strontium, the natural width of the intercombination transition ($\Gamma = 2\pi \times 7.5\,\mathrm{kHz}$) is slightly broader than the recoil shift ($\omega_r = 2\pi \times 4.7\,\mathrm{kHz}$). The radiation pressure force is higher than the gravity but at the same time the final temperature is still in the μK range [7,8]. In parallel, the narrow transition partially prevents multiple scattering processes and the related atomic repulsive force [10]. Hence important improvements on the spatial density have been reported [7]. However, despite experimental efforts, such as adding an extra confining optical potential, pure optical methods have not allowed yet to reach the quantum degeneracy regime with Strontium atoms [9].

In this paper, we will discuss some performances, essentially in terms of temperatures, sizes and loading rates, of a Strontium 88 MOT using the 689 nm ${}^1S_0 \rightarrow {}^3P_1$ intercombination line.

Initially the atoms are precooled in a MOT on the spin-allowed 461 nm ${}^1S_0 \rightarrow {}^1P_1$ transition (natural width $\Gamma = 2\pi \times 32\,\mathrm{MHz}$) as discussed in [11]. Then the atoms are transferred into the 689 nm intercombination MOT. To achieve a high loading rate, Katori et al. [7] have used laser spectrum, broadened by frequency modulation. Thus the velocity capture range of the 689 nm MOT matches the typical velocity in the 461 nm MOT. They report a transfer efficiency of 30%. The same value of transfer efficiency is also reported in reference [8]. In our set-up, 50% of the atoms initially in the blue MOT are transferred into the red one. In section 3 we present a systematic study of the transfer efficiency as function of the parameters of the frequency modulation. In order to discuss the intrinsic limitations of the loading efficiency, we compare our experimental results to a simple model. In particular, we demonstrated that our transfer efficiency is limited by the size of the red MOT beams. We show that it could be optimized up to 90% with realistic laser power (25 mW per beams).

The minimum temperature achieved in the broadband MOT is about 2.5 μK. In order to reduce the temperature down to the photon recoil limit (0.5 μK), we apply a second cooling stage, using a single frequency laser and observe similar temperatures, detuning and intensity dependencies as reported in the literature (see references [7],

[8], [12] and [13]). In those publications, the role of gravity on the cooling and trapping dynamics along the z vertical direction has been discussed. In this paper we compare the steady state behaviour along vertical (z) direction to that along the horizontal plane ($x-y$) where gravity plays indirectly a crucial role (section 4).

Details about the dynamics are given in references [8],[12]. In particular the authors establish three regimes. In regime (I) the laser detuning $|\delta|$ is larger than the power-broadened linewidth $\Gamma_E = \Gamma\sqrt{(1+s)}$. Regime (II) on the contrary corresponds to $\Gamma_E > |\delta|$. In both regimes (I) and (II) $\Gamma_E \gg \Gamma, \omega_r$ and the semiclassical limit is a good approximation. In regime (III) the saturation parameter is small and a full quantum treatment is required. We will focus here on the semiclassical regime (I). In this regime, we confirm that the temperature along the z direction is independent of the detuning δ. Following Loftus et al. [12], we have also found (see section 4.1) that this behavior is due to the balance of the gravitational force and the radiation pressure force produced by the upward pointing laser (the gravity defining the downward direction). The center of mass of the atomic cloud is shifted downward from the magnetic field quadrupole center. As a consequence, cooling and trapping in the horizontal plane occur at a strong bias magnetic field mostly perpendicular to the cooling plane. This unusual situation is studied in detail (section 4.2). Despite different friction and diffusion coefficients along the horizontal and the vertical directions, the horizontal temperature is found to be the same as the vertical one (see section 4.3). In reference [12], the trapping potential is predicted to have a box shape whose walls are given by the laser detuning. This is indeed the case without a bias magnetic field along the z axis. It is actually different for the regime (I) described in this paper. Here we have found that the trapping potential remain harmonic. This leads to a cloud width in the horizontal direction which is proportional to $\sqrt{|\delta|}$ (section 4.2).

2 Experimental set-up

Our blue MOT setup (on the broad $^1S_0 \rightarrow {}^1P_1$ transition at 461 nm) is described in references [14,15]. Briefly, it is composed by six independent laser beams typically $10\,\mathrm{mW/cm^2}$ each. The magnetic field gradient is about 70 G/cm. The blue MOT is loaded from an atomic beam extracted from an oven at 550 °C and longitudinally slowed down by a Zeeman slower. The loading rate of our blue MOT is of 10^9 atoms/s and we trap about 2.10^6 in a 0.6 mm rms radius cloud when no repumping lasers are used [16]. To optimize the transfer into the red MOT, the temperature of the blue MOT should be as small as possible. As previously observed [11], this temperature depends strongly on the optical field intensity. We therefore decrease the intensity by a factor 5 (see figure 1) 4 ms before switching off the blue MOT. The rms velocity right before the transfer stage is thus reduced down to $\sigma_b = 0.6\,\mathrm{m/s}$ whereas the rms size remains unchanged. Similar two stage cooling in a blue MOT is also reported in reference [13].

The 689 nm laser source is an anti-reflection coated laser diode in a 10 cm long extended cavity, closed by a diffraction grating. It is locked to an ULE cavity using the Pound-Drever-Hall technique [17]. The unity gain of the servo loop is obtained at a frequency of 1 MHz. From the noise spectrum of the error signal, we derive a frequency noise power. It shows, in the range of interest, namely 1 Hz − 100 kHz, an upper limit of 160 $\mathrm{Hz^2/Hz}$ which is low enough for our purpose. The transmitted light from the ULE cavity is injected into a 20 mW slave laser diode. Then the noise components at frequencies higher than the ULE cavity cut-off (300 kHz) are filtered. It is important to note that the lateral bands used for the lock-in are also removed. Those lateral bands, at 20 MHz from the carrier, are generated modulating directly the current of the master laser diode. A saturated spectroscopy set-up on the $^1S_0 \rightarrow {}^3P_1$ intercombination line is used to compensate the long term drift of $10-50\,\mathrm{Hz/s}$ mainly due to the daily temperature change of the ULE cavity.

The slave beam is sent through an acousto-optical modulator mounted in a double pass configuration. The laser detuning can then be tuned within the range of a few hundreds of linewidth around the resonance. This acousto-optical modulator is also used for frequency modulation (FM) of the laser, as required during the loading phase (see section 3).

The red MOT is made of three retroreflected beams with a waist of 0.7 cm. The maximum intensity per beam is about $4\,\mathrm{mW/cm^2}$ (the saturation intensity being $I_s = 3\,\mu\mathrm{W/cm^2}$). The magnetic gradient used for the red MOT is varied from 1 to 10 G/cm.

To probe the cloud (number of atoms and temperature) we use a resonant 40 μs pulse of blue light (see fig 1). The total emitted fluorescence is collected onto an avalanche detector. From this measurement, we deduce the number of atoms and then evaluate the transfer rate into the red MOT. At the same time, an image of the cloud is taken with an intensified CCD camera. The typical spatial resolution of the camera is 30 μm. Varying the dark period (time-of-flight) between the red MOT phase and the probe, we get the ballistic expansion of the cloud. We then derive the velocity rms value and the corresponding temperature.

3 Broadband loading of the red MOT

The loading efficiency of a MOT depends strongly on the width of the transition. With a broad transition, the maximum radiation pressure force is typically $a_m = \frac{v_r\Gamma}{2} \approx 10^4 \times g$, where v_r is the recoil velocity [18]. Hence, on $l \approx 1\,\mathrm{cm}$ (usual MOT beam waist) an atom with a velocity $v_c = \sqrt{2a_m l} \approx 30\,\mathrm{m/s}$ can be slowed down to zero and then be captured. During the deceleration, the atom remains always close to resonance because the Doppler shift is comparable to the linewidth. Thus MOTs can be directly loaded from a thermal vapor or a slow atomic beam using single frequency lasers. Moreover typical magnetic field gradients of few tens of G/cm usually do not dras-

tically change the loading because the Zeeman shift over the trapping region is also comparable to the linewidth.

An efficient loading is more complex to achieved with a narrow transition. For Strontium, the maximum radiation pressure force of a single laser is only $a_m \approx 15 \times g$. Assuming the force is maximum during all the capture process, one gets $v_c = \sqrt{2a_m l} \approx 1.7\,\mathrm{m/s}$. Hence, precooling in the blue MOT is almost mandatory. In that case the initial Doppler shift will be $v_c\lambda^{-1} \approx 2.5\,\mathrm{MHz}$, 300 times larger than the linewidth. In order to keep the laser on resonance during the capture phase, the red MOT lasers must thus be spectrally broadened. Because of the low value of the saturation intensity, the spectral power density can easily be kept large enough to maintain a maximum force with a reasonable total power (few milliwatts). The magnetic field gradient of the MOT may also affect the velocity capture range. To illustrate this point, let us consider an atom initially in the blue MOT at the center of the trap with a velocity $v_c = 1.7\,\mathrm{m/s}$. During the deceleration, the Doppler shift decreases whereas the Zeeman shift increases. However, the magnetic field gradient does not affect the capture velocity as far as the total shift (Doppler+Zeeman) is still decreasing. This condition is fulfilled if the magnetic field gradient is lower than [19]:

$$b_c = \frac{a_m}{\lambda g_e \mu_b v_c} \approx 0.6\,\mathrm{G/cm} \qquad (1)$$

where $g_e = 1.5$ is the Landé factor of the $^3P_1$ level and $\mu_b = 1.4\,\mathrm{MHz/G}$ is the Bohr magneton. In practice we use a magnetic field gradient which is larger than b_c. In that case, it is necessary to increase the width of the laser spectrum so that the optimum transfer rate is not limited by the Zeeman shift (see section 3.2). An alternative solution may consist of ramping the magnetic field gradient during the loading [7].

3.1 Transfer rate: experimental results

In this section we will present the experimental results regarding the loading efficiency of the red MOT from the blue MOT. To optimize the transfer rate, the laser spectrum is broadened using frequency modulation (FM). Thus the instantaneous laser detuning is $\Delta(t) = \delta + \Delta\nu.\sin\nu_m t$. $\Delta\nu$ and ν_m are the frequency deviation and modulation frequency respectively, δ is the carrier detuning. Here, the modulation index $\Delta\nu/\nu_m$ is always larger than 1, thus the so-called wideband limit is well fulfilled. Hence one can assume the FM spectrum to be mainly enclosed in the interval $[\delta - \Delta\nu; \delta + \Delta\nu]$.

As shown in figure 2, the transfer rate increases with ν_m up to 15 kHz where we observe a plateau at 45% transfer efficiency. On the one hand when ν_m is larger than the linewidth, the atoms are in the non-adiabatic regime where they interact with all the Fourier components of the laser spectrum. Moreover, the typical intensity per Fourier component remains always higher than the saturation intensity $I_s = 3\,\mu\mathrm{W/cm^2}$. As a consequence, the radiation pressure force should be close to its maximum value for any atomic velocity. On the other hand when $\nu_m < \Gamma/2\pi$, the atoms interact with a chirped intense laser where the mean radiation pressure force (over a period $2\pi/\nu_m$) is clearly smaller than in the case $\nu_m > \Gamma/2\pi$. As a consequence, the transfer rate is reduced when ν_m decreases.

In figure 3, the transfer rate is measured as a function of $\Delta\nu$. The carrier detuning is $\delta = -1\,\mathrm{MHz}$ and the modulation frequency is kept larger than the linewidth ($\nu_m = 25\,\mathrm{kHz}$). Starting from no deviation ($\Delta\nu = 0$), we observe (fig. 3) an increase of the transfer rate with $\Delta\nu$ (in the range $0 < \Delta\nu < 500\,\mathrm{kHz}$). After reaching its maximum value, the transfer rate does not depend on $\Delta\nu$ anymore. Thus the capturing process is not limited by the laser spectrum anymore. If we further increase the frequency deviation $\Delta\nu$, the transfer becomes less efficient and finally decreases again down to zero. This reduction occurs as soon as $\Delta\nu > |\delta|$, *i.e.* some components of the spectrum are blue detuned. This frequency configuration obviously should affect the MOT steady regime adding extra heating at zero velocity (see section 3.3). We can see that it is also affecting the transfer rate. To confirm that point, figure 4 shows the same experiment but with a larger detuning $\delta = -1.5\,\mathrm{MHz}$ and $\delta = -2\,\mathrm{MHz}$ for the figures 4a and 4b respectively. Again the transfer rate decreases as soon as $\Delta\nu > |\delta|$. The transfer rate is also very small on the other side for small values of $\Delta\nu$. In that case the entire spectrum of the laser is too far red detuned. The radiation pressure forces are significant only for velocities larger than the capture velocity and no steady state is expected. Keeping now the deviation fixed and varying the detuning as shown in figure 5, we observe a maximum transfer rate when the detuning is close to the deviation frequency $\Delta\nu \simeq |\delta|$. Closer to resonance ($\Delta\nu < |\delta|$), the blue detuned components prevent an efficient loading of the MOT.

The magnetic field gradient plays also a crucial role for the loading. We indeed observe (fig. 6) that the transfer rate decreases when the magnetic field gradient increases. At very low magnetic field ($b < 1\,\mathrm{G/cm}$) the reduction of the transfer rate is most likely due to a lack of stability within the trapping region. In that case we actually observe a strong displacement of the center of mass of the cloud. This is induced by imperfections of the set-up such as non-balanced laser intensities which are critical at low magnetic gradient. Hence, the optimum magnetic field gradient is found to be the smallest one which ensure the stability of the cloud in the MOT.

3.2 Theoretical model and comparison with the experiments

To clearly understand the limiting processes of the transfer rate, we compare the experimental data to a simple 1D theoretical model based on the following assumptions:
- An atom undergoes a radiation pressure force and thus a deceleration if the modulus of its velocity is between v_{max} and v_{min} with

$$v_{max} = \lambda(|\delta| + \Delta\nu), \quad v_{min} = \max\{\lambda(|\delta| - \Delta\nu); \lambda(-|\delta| + \Delta\nu)\} \qquad (2)$$

$a_m = 0$ elsewhere. We simply write that the Doppler shift is contained within the FM spectrum. We add the condition $v_{min} = \lambda(-|\delta| + \Delta\nu)$ when some components are blue detuned $\Delta\nu > |\delta|$. In this case, we consider the simple ideal situation where the two counter-propagating lasers are assumed perfectly balanced and then compensate each other in the spectral overlapping region.
- Even in the semiclassical model, it is difficult to calculate the acceleration as a function of the velocity for a FM spectrum. However for all the data presented here, the saturation parameter is larger than one. Hence the deceleration is set to a constant value $-\frac{1}{3}a_m$ when $v_{min} < |v| < v_{max}$. The prefactor 1/3 takes into account the saturation by the 3 counter-propagating laser beam pairs.
- The magnetic field gradient is included by giving a spatial dependence of the detuning δ in the expression (2).
- An atom will be trapped if its velocity changes of sign within a distance shorter that the beam waist.

In figures 3-6 the results of the model are compared to the experimental data. The agreement between the model and the experimental data is correct except at large frequency deviation (figures 3 and 4) or at low detuning (figure 5). In those cases the spectrum has some blue detuned components. As mentionned before, this is a complex situation where the assumptions of the simple model do not hold anymore. Fortunately those cases do not have any practical interest because they do not correspond to the optimum transfer efficiency.

At the optimum, the model suggests that the transfer is limited by the beam waist (see caption of figures (3-6)). Moreover for all the situation explored in figures 3-5, the magnetic field gradient is strong enough ($b = 1\,\mathrm{G/cm}$) to have an impact on the capture process, as suggested by the inequality (1). However it is not the transfer limiting factor because the Zeeman shift is easily compensated by a larger frequency excursion or by a larger detuning.

Increasing the beam waist would definitely improve the transfer efficiency as showed in figure 7. If the saturation parameter would remain large for all values of beam waist, more than 90% of the atoms would be transferred for a 2 cm beam waist. 25 mW of power per beam should be sufficient to achieve this goal. In our experimental set-up, the power is limited to 3 mW per beam. So the saturation parameter is necessarily reduced once the waist is increased. To take this into account and get a more realistic estimation of the efficiency for larger beams, we replace the previous acceleration by the expression $a_m s/(1+3s)$, with $s = I/I_s$ the saturation parameter per beam. In this case, the transfer efficiency becomes maximum at 70% for a beam waist of 1.5 cm.

3.3 Temperature

Cooling with a broadband FM spectrum on the intercombiaison line decreases the temperature by three orders of magnitude in comparison with the blue MOT: from 3 mK ($\sigma_b = 0.6\,\mathrm{m/s}$) to 2.5 μK (see figure 8). For small detuning, the temperature is strongly increasing when the spectrum has some blue detuned components ($\Delta\nu > |\delta|$). Indeed the cooling force and heating rate are strongly modified at the vicinity of zero detuning. This effect is illustrated in figure 8. On the other side at large detuning ($\delta < -1.5\,\mathrm{MHz}$), the temperature becomes constant. This regime corresponds to a detuning independent steady state, as also observed in single frequency cooling (see ref. [12] and section 4).

4 Single frequency cooling

About half of the atoms initially in the 461 nm MOT are recaptured in the red one using a broadband laser. The final temperature is 2.5 μK *i.e.* 5 times larger than the photon recoil temperature $T_r = 460\,\mathrm{nK}$. To further decrease the temperature one has to switch to single frequency cooling (for time sequences: see figure 1). As we will see in this section, the minimum temperature is now about 600 nK close to the expected $0.8T_r$ in an 1D molasses [5]. Moreover, one has to note that, under proper conditions described in reference [12], the transfer between the broadband and the single frequency red MOT can be almost lossless.

In the steady state regime of the single frequency red MOT, one has $k\sigma_v \approx \omega_r \approx \Gamma$. Thus, there is no net separation of different time scales as in MOTs operated with a broad transition where $\omega_r << k\sigma_v << \Gamma$. However, here the saturation parameter s always remains high. It corresponds to the so-called regimes (I) and (II) presented in reference [12]. Thus $\omega_r << \Gamma\sqrt{1+s}$ and the semiclassical Doppler theory describes properly the encountered experimental situations.

To insure an efficient trapping, the parameter's values of the single frequency red MOT are different from a usual broad transition MOT: the magnetic field gradient is higher, typically $1000\Gamma/cm$. Moreover the gravity is not negligible anymore by comparison with the typical radiation pressure. Those features lead to an unusual behavior of the red MOT as we will explain in this section. We will first independently analyze the MOT properties along the vertical dimension (section 4.1) then in the horizontal plane (section 4.2), to finally compare those two situations (section 4.3).

4.1 Vertical direction

In the regime (I) *i.e.* at large negative detuning and high saturation (see examples on figure 9a) the temperature is indeed constant. As explained in reference [12], this behavior is due to the balance between the gravity and the radiation pressure force of the upward laser. At large negative detuning, the downward laser is too far detuned to give a significant contribution. In the semiclassical regime, an atom undergoes a net force of

$$F_z = \hbar k \frac{\Gamma}{2} \frac{s}{1 + s_T + 4(\delta - g_e \mu_B b z - k v_z)^2/\Gamma^2} - mg \quad (3)$$

Considering the velocity dependence of the force, the first order term is:

$$F_z \approx -\gamma_z v_z \tag{4}$$

with

$$\gamma_z = -4\frac{\hbar k^2 \delta_{\text{eff}}}{\Gamma}\frac{s}{(1+s_T+4\delta_{\text{eff}}^2/\Gamma^2)^2} \tag{5}$$

where the effective detuning $\delta_{\text{eff}} = \delta - g_e\mu_B b < z >$ is define such as

$$\hbar k\frac{\Gamma}{2}\frac{s}{1+s_T+4\delta_{\text{eff}}^2/\Gamma^2} = mg \tag{6}$$

s_T is the total saturation parameter including all the beams. $< z >$ is the mean vertical position of the cold cloud. Hence δ_{eff} is independent of the laser detuning δ and the vertical temperature at larger detuning depends only on the intensity as shown in figures 9a and 9b.

The spatial properties of the cloud are also related to the effective detuning δ_{eff} which is independent of δ. The mean vertical position depends linearly on the detuning, so that one has :

$$\frac{\mathrm{d} < z >}{\mathrm{d}|\delta|} = \frac{-1}{g_e\mu_B b} \tag{7}$$

The predicted vertical displacement is compared to the experimental data in figure 10a. The agreement is excellent (the only adjustable parameter is the unknown origin of the vertical axe). Because the radiation pressure force for an atom at rest does not depend on the laser detuning δ, the vertical rms size should be also δ-independent. This point is also verified experimentally (see figure 10b).

4.2 $x-y$ horizontal plane

Let us now study the behavior of the cold cloud in the $x-y$ plane at large laser detuning. As explained in section 4.1, the position of the cloud is vertically shifted downward with respect to the center of the magnetic field quadrupole (see figure 11). The dynamic in the $x-y$ plane occurs thus in the presence of a high bias magnetic field. To derive the expression of the semiclassical force in this unusual situation one has first to project the circular polarizations states of the horizontal lasers on the eigenstates. We define the quantification axis along the magnetic field, one gets:

$$e_x^+ = \frac{1+\sin\alpha}{2}e_B^- + \frac{\cos\alpha}{\sqrt{2}}\pi_B + \frac{1-\sin\alpha}{2}e_B^+ \tag{8}$$

$$e_x^- = \frac{1-\sin\alpha}{2}e_B^- + \frac{\cos\alpha}{\sqrt{2}}\pi_B + \frac{1+\sin\alpha}{2}e_B^+ \tag{9}$$

where e_i^-, π_i and e_i^+ represent respectively the left-handed, linear and right-handed polarisations along the i axis. The angle α between the vertical axis and the local magnetic field is shown on figure 11. For large detuning, α is always small ($\alpha \ll 1$) and we write $\alpha \approx -x/ < z >$ considering only the dynamics along the x dimension. For simplicity the magnetic field gradient b is considered as spatially isotropic with $b > 0$ as sketched on figure 11b. The expression of the radiation pressure force is then:

$$F_x = \hbar k\frac{\Gamma}{2}(\frac{s(1-\sin\alpha)^2/4}{1+s_T+4(\delta-g_e\mu_B b < z > (1-\tan\alpha)-kv_x)^2/\Gamma^2} - \frac{s(1+\sin\alpha)^2/4}{1+s_T+4(\delta-g_e\mu_B b < z > (1-\tan\alpha)+kv_x)^2/\Gamma^2}) \tag{10}$$

Note that this expression is not restricted to the small α values. We expect six terms in the expression (11): three terms for each laser corresponding to the three e_B^-, π_B and e_B^+ polarisation eigenstates. However only two terms, corresponding to the e_B^+ state, are close to resonance and thus have a dominant contribution. As for the vertical dimension, the off resonant terms are removed from the expression (11). One has also to note that the effective detuning $\delta_{\text{eff}} = \delta - g_e\mu_B b < z >$ is actually the same as the one along the vertical dimension.

The first order expansion of (11) in α and kv_x/Γ gives the expression of the horizontal radiation pressure force:

$$F_x \approx -\kappa_\alpha\alpha - \gamma_x v_x = -\kappa_x x - \gamma_x v_x \tag{11}$$

with

$$\kappa_\alpha = - < z > \kappa_x = \hbar k\frac{\Gamma}{2}\frac{s}{1+s_T+4\delta_{\text{eff}}^2/\Gamma^2} = mg \tag{12}$$

and

$$\gamma_x = \frac{\gamma_z}{2} = -2\frac{\hbar k^2\delta_{\text{eff}}}{\Gamma}\frac{s}{(1+s_T+4\delta_{\text{eff}}^2/\Gamma^2)^2} \tag{13}$$

As for the vertical dimension (equation (6)), the force depends on δ_{eff} but at the position of the MOT does not depend on the laser detuning δ. Hence, at large detuning, the horizontal temperature depends only on the intensity as observed in figures 9a and 9b.

To understand the trapping mechanisms in the $x-y$ plane, we now consider an atom at rest located at a position $x \neq 0$ (corresponding to $\alpha \neq 0$), i.e. not in the center of the MOT. The transition rate of two counter-propagating laser beam is not balanced anymore. This is due to the opposite sign in the α dependency of the prefactor in expression (11). This mechanism leads to a restoring force in the $x-y$ plane at the origin of the spatial confinement (equation 11). Applying the equipartition theorem one gets the horizontal rms size of the cloud:

$$x_{\text{rms}}^2 = \frac{k_B T}{\kappa_x} = -\frac{< z > k_B T}{mg} \tag{14}$$

Without any free adjusting parameter, the agreement with experimental data is very good as shown in figure 10b. On the other hand there's no displacement of the center of mass in the $x-y$ plane whatever is the detuning δ as long as the equilibrium of the counter-propagating beams intensities is preserved (figure 10a).

4.3 Comparing the temperatures along horizontal and vertical axes

As seen in sections 4.1 and 4.2, gravity has a dominant impact on cooling in a MOT operated on the intercombination line not only along the vertical axe but also in the horizontal plane. Even so we expect different behaviors along this directions essentially because the gravity renders the trapping potential anisotropic. This is indeed the case for the spatial distribution (figures 10a and 10b) whereas the temperatures are surprisingly the same (figures 9a and 9b). We will now give few simple arguments to physically explain this last point.

In the semiclassical approximation, the temperature is defined as the ratio between the friction and the diffusion term:

$$k_B T_i = \frac{\gamma_i}{D_i^{abs} + D_i^{spo}} \quad \text{with} \quad i = x, y, z \tag{15}$$

D^{abs} and D^{spo} correspond to the diffusion coefficients induced by absorption and spontaneous emission events respectively. The friction coefficients has been already derived (equation 13):

$$\gamma_z = 2\gamma_{x,y} \tag{16}$$

Indeed cooling along an axe in the $x-y$ plane results in the action of two counter-propagating beams four times less coupled than the single upward laser beam. The same argument holds for the absorption term of the diffusion coefficient:

$$D_z^{abs} = 2D_{x,y}^{abs} \tag{17}$$

The spontaneous emission contribution in the diffusion coefficient can be derived from the differential cross-section $\mathrm{d}\sigma/\mathrm{d}\Omega$ of the emitting dipole [20]. With a strong biased magnetic field along the vertical direction, this calculation is particularly simple as e_z^+ is the only quasi resonant state. Hence

$$\mathrm{d}\sigma/\mathrm{d}\Omega \propto (1 + \cos\phi^2) \tag{18}$$

ϕ is the angle between the vertical axe and the direction of observation. After a straightforward integration, one finds a contribution again two times larger along the vertical axe:

$$D_z^{spo} = 2D_{x,y}^{spo} \tag{19}$$

From those considerations, the temperature is expected to be isotropic as observed experimentally (see figures 9a and 9b).

In the so-called regime (I), the minimum temperature is given by the semiclassical Doppler theory:

$$T = N_R \frac{\hbar\Gamma}{2k_B}\sqrt{s} \tag{20}$$

Where N_R is a numerical factor which should be close to two [12]. This solution is represented in figure 9 by a dashed line nicely matching the experimental data for $s > 8$ but with $N_R = 1.2$. Similar results, *i.e.* with unexpected low N_R values, have been found in [12]. For $s \leq 8$ we observed a plateau in the final temperature slightly higher than the low saturation theoretical prediction [5]. We cannot explain why the temperature does not decrease further down as reported in [12]. For quantitative comparison with the theory, more detailed studies in a horizontal 1D molasses are required.

4.4 Conclusions

Cooling of Strontium atoms using the intercombination line is an efficient technique to reach the recoil temperature in three dimensions by optical methods. Unfortunately loading from a thermal beam cannot be done directly with a single frequency laser because of the narrow velocity capture range. We have shown experimentally that more than 50% of the atoms initially in a blue MOT on the dipole-allowed transition are recaptured in the red MOT using a frequency-broadened spectrum. Using a simple model, we conclude that the transfer is limited by the size of the laser beam. If the total power of the beams at 689 nm was higher, transfer rates up to 90% could be expected by tripling our laser beam size. The final temperature in the broadband regime is found to be as low as 2.5 μK, *i.e.* only 5 times larger than the photon recoil temperature. The gain in temperature by comparison to the blue MOT ($1-10$ mK) is appreciable. So in absence of strong requirements on the temperature, broadband cooling is very efficient and reasonably fast (less than 100 ms). The requirements for the frequency noise of the laser are also much less stringent than for single frequency cooling.

Using a subsequent single frequency cooling stage, it is possible to reduce the temperature down to 600 nK, slightly above the photon recoil temperature. Analyzing the large detuning regime, we particularly focus our studies on the comparison between vertical and horizontal directions. We show how gravity indirectly influences the horizontal parameters of the steady state MOT and find that the trapping potential remains harmonic along all directions, but with an anisotropy.

Gravity has a major impact on the MOT as it counterbalances the laser pressure of the upward laser (making the steady state independent of the detuning). We show that gravity thus affects the final temperature, which remains isotropic, despite different cooling dynamics along the vertical and horizontal directions.

5 Acknowledgments

The authors wish to thank J.-C. Bernard and J.-C. Bery for valuable technical assistances. This research is financially supported by the CNRS (Centre National de la Recherche Scientifique) and the former BNM (Bureau National de Métrologie) actually LNE (Laboratoire national de métrologie et d'essais) contract N° 03 3 005.

References

1. F. Ruschewitz, J. L. Peng, H. Hinderthr, N. Schaffrath, K. Sengstock, and W. Ertmer, Phys. Rev. Lett. **80**, 3173 (1998); G. Ferrari, P. Cancio, R. Drullinger, G. Giusfredi, N. Poli, M. Prevedelli, C. Toninelli, and G. M. Tino Phys. Rev. Lett. **91**, 243002 (2003); M. Yasuda and H. Katori Phys. Rev. Lett. **92**, 153004 (2004); T. Ido, T. H. Loftus, M. M. Boyd, A. D. Ludlow, K. W. Holman, and J. Ye Phys. Rev. Lett. **94**, 153001 (2005); R. Le Targat, X. Baillard, M. Fouch, A. Brusch, O. Tcherbakoff, G. D. Rovera, and P. Lemonde Phys. Rev. Lett. **97**, 130801 (2006).
2. J. Weiner, V. Bagnato, S. Zilio, and P. S. Julienne, Rev. Mod. Phys. **71**, 1 (1999); T. Dinneen, K. R. Vogel, E. Arimondo, J. L. Hall, and A. Gallagher, Phys. Rev. A **59**, 1216 (1999). A.R.L.Caires, G.D.Telles, M.W.Mancini, L.G.Marcassa, V.S.Bagnato, D.Wilkowski, R. Kaiser, Bra. J. Phys. **34**, 1504 (2004).
3. M. M. Boyd, T. Zelevinsky, A. D. Ludlow, S.M. Forman, T. Ido, and J. Ye Science **314**, 1430 (2006).
4. D. Hayes, P. Julienne, I. Deutsch, Arxiv, quant-ph/0609111.
5. Y. Castin, H. Wallis, and J. Dalibard, J. Opt. Soc. Am. B. **6**, 2046 (1989).
6. T. Binnewies, G. Wilpers, U. Sterr, F. Riehle, and J. Helmcke, T. E. Mehlstubler, E. M. Rasel, and W. Ertmer, Phys. Rev. Lett. **87**, 123002 (2001).
7. H. Katori, T. Ido, Y. Isoya, and M. Kuwata-Gonokami, Phys. Rev. Lett. **82**, 1116 (1999)
8. T. H. Loftus, T. Ido, A. D. Ludlow, M. M. Boyd, and J. Ye, Phys. Rev. Lett. **93**, 073003 (2004).
9. T. Ido, Y. Isoya, and H. Katori, Phys. Rev. A **61**, 061403 (2000).
10. D. W. Sesko, T. G. Walker and C. E. Wieman, J. Opt. Soc. Am. B **8**, 946 (1991).
11. T. Chanelière, J.-L. Meunier, R. Kaiser, C. Miniatura, and D. Wilkowski. J. Opt. Soc. Am. B, **22**, 1819 (2005).
12. T. H. Loftus, T. Ido, M. M. Boyd, A. D. Ludlow, and J. Ye, Phys. Rev. A **70**, 063413 (2004).
13. K. R. Vogel, Ph. D. Thesis, University of Colorado, Boulder, CO 80309, (1999).
14. Y. Bidel, B. Klappauf, J.C. Bernard, D. Delande, G. Labeyrie, C. Miniatura, D. Wilkowski, R. Kaiser, Phys. Rev. Lett. **88**, 203902 (2002).
15. B. Klappauf, Y. Bidel, D. Wilkowski, T. Chanelière, R. Kaiser, Appl.Opt. **43**, 2510 (2004).
16. D. Wilkowski, Y. Bidel, T. Chanelière, R. Kaiser, B. Klappauf, C. Miniatura, SPIE Proceeding **5866**, 298 (2005).
17. N. Poli, G. Ferrari, M. Prevedelli, F. Sorrentino, R. E. Drullinger, and G. M. Tino, Spectro. Acta Part A **63**, 981 (2006).
18. H.J. Metcalf, P. van der Straten, Laser cooling and trapping, Springer, (1999).
19. C. Dedman, J. Nes, T. Hanna, R. Dall, K. Baldwin, and A. Truscott, Rev. Mod. Phys., **75**, 5136 (2004).
20. J.D. Jackson, *Classical Electrodynamics* (J. Wiley and sons, third edition New York, 1999).

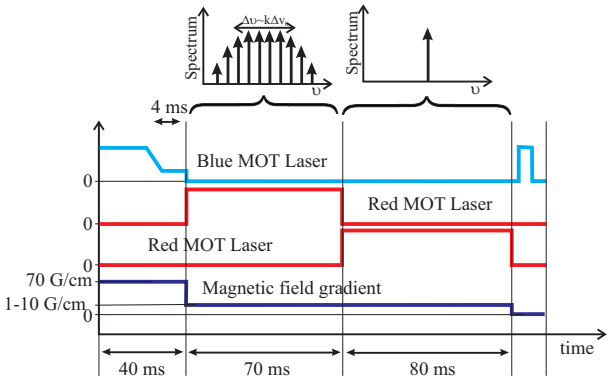

Fig. 1. Time sequence and cooling stages of Strontium with the dipole-allowed transition and with the intercombination line.

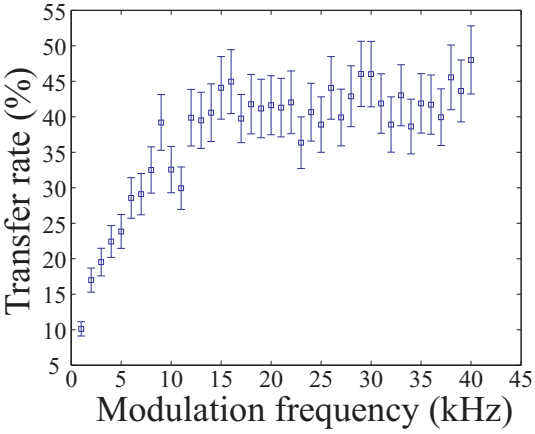

Fig. 2. Transfer rate as a function of the modulation frequency. The other parameters are fixed: $P = 3\,\mathrm{mW}$, $\delta = -1000\,\mathrm{kHz}$, $b = 1\,\mathrm{G/cm}$ and $\Delta\nu = 1000\,\mathrm{kHz}$

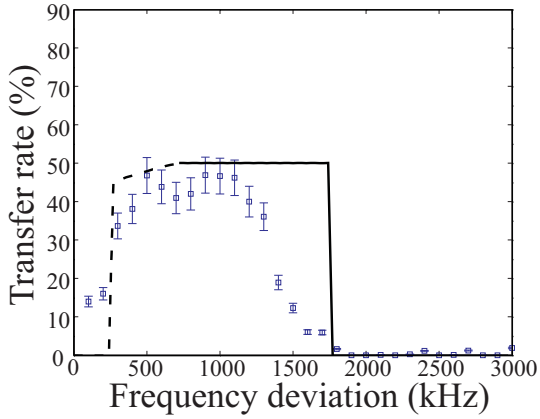

Fig. 3. Transfer rate as a function of the frequency deviation (squares). The other parameters are fixed: $P = 3\,\mathrm{mW}$, $\delta = -1000\,\mathrm{kHz}$, $b = 1\,\mathrm{G/cm}$ and $\nu_m = 25\,\mathrm{kHz}$. The dash and solid line correspond to a simple model prediction (see text). The transfer rate is limited by the frequency deviation of the broad laser spectrum for the dash line and by the waist of the MOT beam for the solid line.

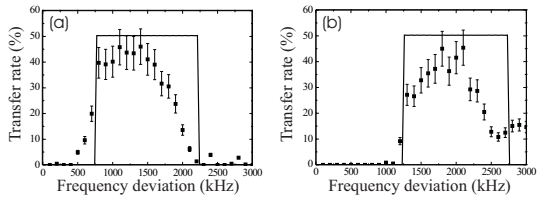

Fig. 4. Transfer rate as a function of the frequency deviation (squares). $\delta = -1500\,\mathrm{kHz}$ and $\delta = -2000\,\mathrm{kHz}$ for (a) and (b) respectively, the other parameters and the definitions are the same than for figure 3.

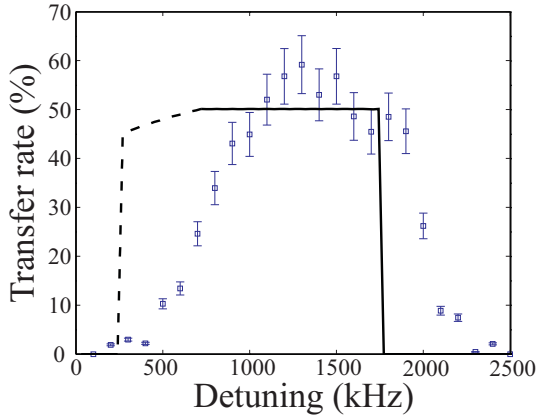

Fig. 5. Transfer rate as a function of the detuning (squares). The other parameters are fixed: $P = 3\,\mathrm{mW}$, $\Delta\nu = 1000\,\mathrm{kHz}$, $b = 1\,\mathrm{G/cm}$ and $\nu_m = 25\,\mathrm{kHz}$. The dashed and solid lines have the same signification than in figure 3.

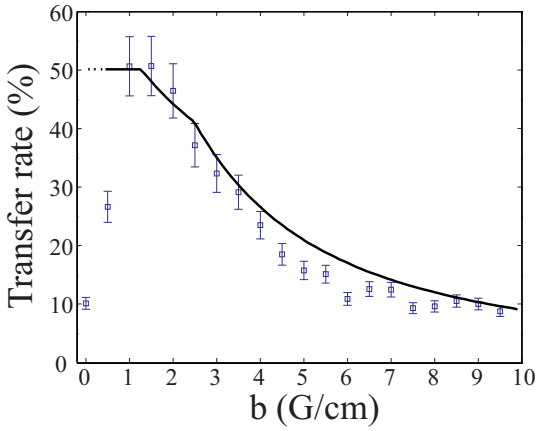

Fig. 6. Transfer rate as a function of the magnetic gradient (squares). The other parameters are fixed: $P = 3\,\mathrm{mW}$, $\delta = -1000\,\mathrm{kHz}$, $\Delta\nu = 1000\,\mathrm{kHz}$ and $\nu_m = 25\,\mathrm{kHz}$. The transfer rate is limited by the waist of the MOT beam for all values. The dotted lines represent the case where the magnetic field gradient do not affect the deceleration.

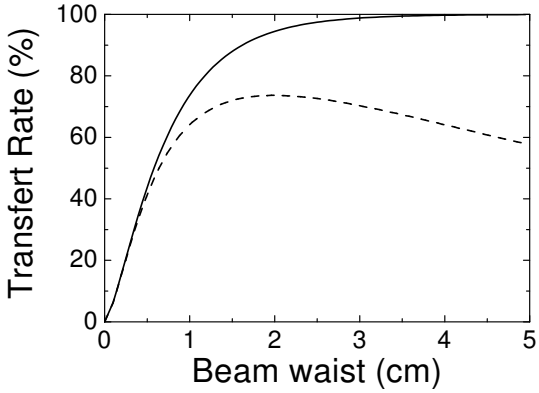

Fig. 7. Transfer rate as a function of the beam waist. The solid lines correspond to a high saturation parameter where as the dash line correspond to a constant power of $P = 3\,\mathrm{mW}$. The other parameters are fixed: $\delta = -1000\,\mathrm{kHz}$, $\Delta\nu = 1000\,\mathrm{kHz}$ and $b = 0.1\,\mathrm{G/cm}$.

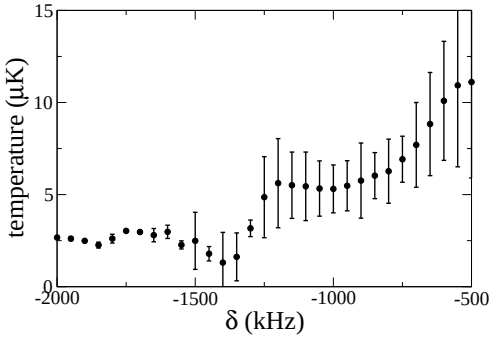

Fig. 8. Measured temperature as a function of the detuning for a FM spectrum. The other parameters are fixed: $P = 3\,\mathrm{mW}$, $b = 1\,\mathrm{G/cm}$, $\Delta\nu = 1000\,\mathrm{kHz}$ and $\nu_m = 25\,\mathrm{kHz}$

.

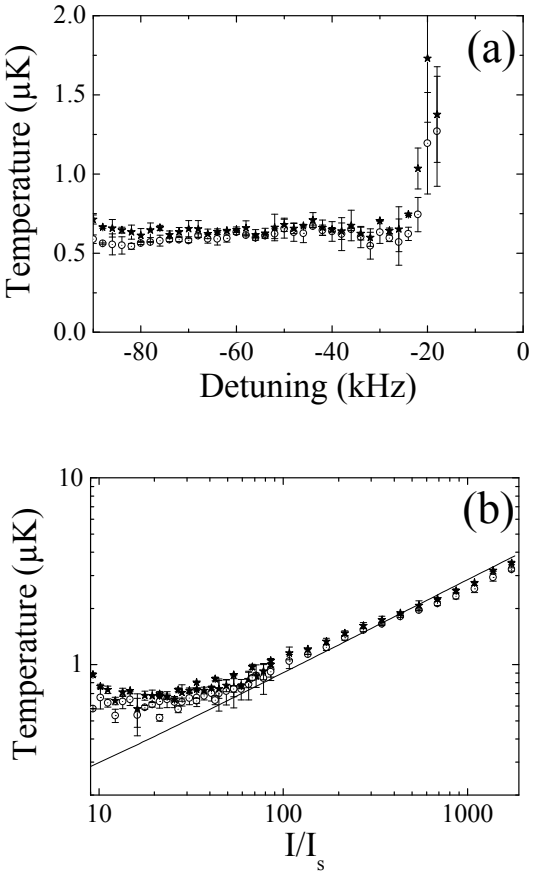

Fig. 9. Measured temperature as a function of the detuning (a) with $I = 4I_s$ or $I = 15I_s$ and as a function of the intensity (b) with $\delta = -100\,\mathrm{kHz}$ of single frequency cooling. The circles (respectively stars) correspond to temperature along one of the horizontal (respectively vertical) axis. The magnetic field gradient is $b = 2.5\,\mathrm{G/cm}$

.

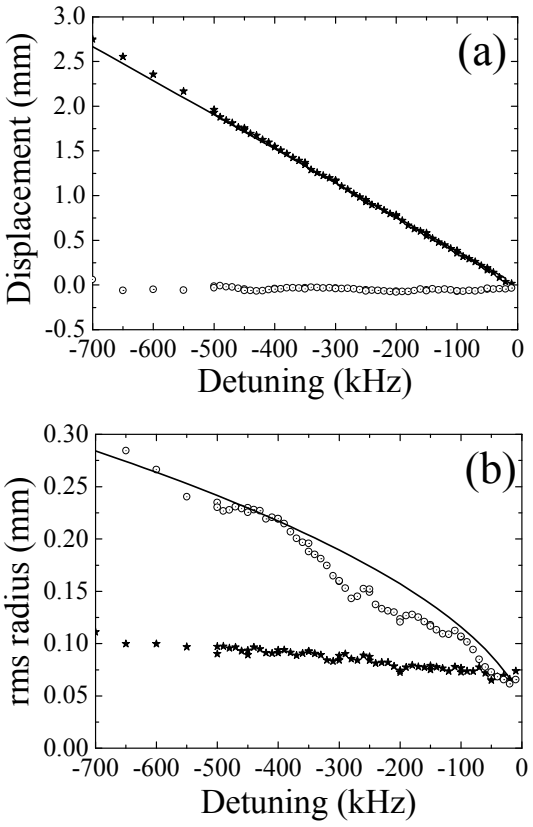

Fig. 10. Displacement (a) and rms radius (b) of the cold cloud in single frequency cooling along the z axis (star) and in the $x-y$ plane (circle). The intensity per beam is $I = 20I_s$ and the magnetic gradient $b = 2.5\,\mathrm{G/cm}$ along the strong axis in the $x-y$ plane. The linear displacement prediction correspond to the plain line (graph a). In graph b, the plain curve correspond to the rms radius prediction based on the equipartition theorem.

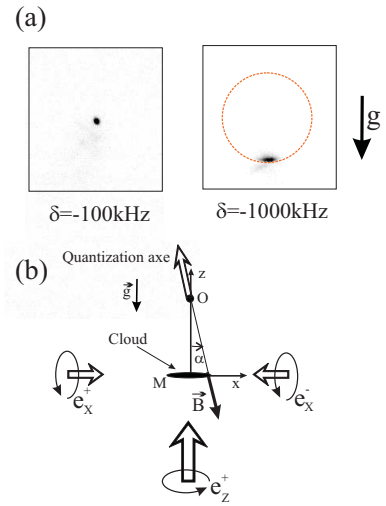

Fig. 11. (a) Images of the cold cloud in the red MOT. The cloud position for $\delta = -100\,\mathrm{kHz}$ coincides roughly with the center of the MOT whereas it is shifted downward for $\delta = -1000\,\mathrm{kHz}$. The spatial position of the resonance correspond dot circle. (b) Sketch representing the large detuning case. The coupling efficiency of the MOT lasers is encoded in the size of the empty arrow. The laser form below has maximum efficiency whereas the one pointing downward is absent because is too detuned. Along a horizontal axe, the lasers are less coupled because they do not have the correct polarization. The α angle is the angular position of an atom M with respect to O, the center of the MOT.